Computational Discovery and Characterization of New B_2O Phases

Jianyun Wang,[a] Quan Li,[a,*] Chris J. Pickard,[b,c] Changfeng Chen,[d] and Yanming Ma[a,*]

[a]*State Key Laboratory of Superhard Materials, Key Laboratory of Automobile Materials of MOE, Innovation Center for Computational Physics Method and Software, and Department of Materials Science, Jilin University, Changchun 130012, China*

[b]*Department of Materials Science and Metallurgy, University of Cambridge, 27 Charles Babbage Road, Cambridge CB3 0FS, United Kingdom*

[c]*Advanced Institute for Materials Research, Tohoku University 2-1-1 Katahira, Aoba, Sendai, 980-8577, Japan*

[d]*Department of Physics and Astronomy, University of Nevada, Las Vegas, Nevada 89154, USA*

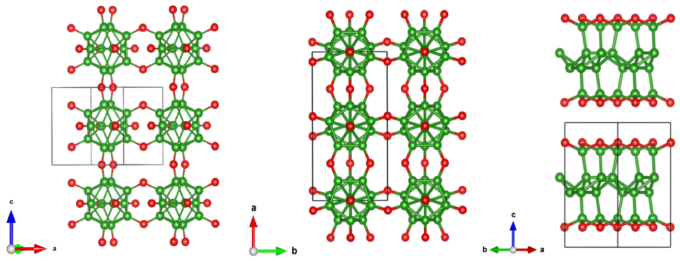

TOC

Our theoretical investigations have unraveled peculiar bonding characters in the current identified superconducting phases for B_2O at high pressure, especially the evolution of chemical bonds and electronic states associated with the B_{12} icosahedral unit in the orthorhombic phase and the pseudo-layered trigonal phase.

Abstract

We present computational discoveries of new structural phases of B_2O compound exhibiting novel bonding networks and electronic states at ambient and elevated pressures. Our advanced crystal structure searches in conjunction with density functional theory calculations have identified an orthorhombic phase of B_2O that is energetically stable at ambient pressure and contains an intriguing bonding network of icosahedral B_{12} clusters bridged by oxygen atoms. As pressure increases above 1.9 GPa, a structural transformation takes the orthorhombic B_2O into a pseudo-layered trigonal phase. We have performed extensive studies to investigate the evolution of chemical bonds and electronic states associated with the B_{12} icosahedral unit in the orthorhombic phase and the covalent B-O bonds in the trigonal phase. We also have examined the nature of the charge carriers and their coupling to the lattice vibrations in the newly identified B_2O crystals. Interestingly, our results indicate that both B_2O phases become superconducting at low temperatures, with transition temperatures of 6.4 K and 5.9 K, respectively, in the ambient and high-pressure phase. The present findings establish new B_2O phases and characterize their structural and electronic properties, which offer insights and guidance for exploration toward further fundamental understanding and potential synthesis and application.

KEYWORDS: CALYPSO, High Pressure, Crystal structure, Multicentral bonds, Superconducting

I. Introduction

Boron possesses strong bonding abilities in forming diverse variety of compounds, and has attracted great attention in the fields of physics, chemistry and materials science. Elemental boron is on the borderline between metals and nonmetals in the Periodic Table and adopts a rich and intricate variety of crystal structures with unusual and complex covalent bonds.[1] Boron has three bonding electrons, which, in most cases, are insufficient to form sp^3 hybridization accompanied by an unoccupied *p* orbital, and thus it has a characteristic electron-deficient nature. In particular, boron is inclined to form three-center two-electron (3*c*-2*e*) bonds in triangular planes within a molecular-like twelve-atom cluster (B_{12}) of approximate icosahedral symmetry, instead of the conventional two-center two-electron (2*c*-2*e*) bonds. The striking nonmetallic characteristics of boron originate from the formation of three-center bonds in crystalline states within a molecular-like icosahedron and among three icosahedra to compensate for its electron deficiency. Such fascinating icosahedral clusters are also usually found in boron-rich compounds, e.g., B_4C, B_6O, $B_{12}As_2$, and $B_{12}P_2$. [2-8]

Although common morphological features based on the B_{12} icosahedron include a twelve-atom cluster with each boron atom located on the vertex of the icosahedron, the bonding networks and electronic states are very sensitive to changes in chemical composition. The covalent bonding distribution in the framework of B_{12} in α-B involves 13 internal bonding orbitals and 12 external bonding connected by direct bonding or through additional atoms.[9,10] The rationalized description of chemical bonds in γ-boron comprises 2*c*-2*e* and 3*c*-2*e* in the packing of the B_{12} cluster and B_2 dumbbells in a distorted cubic arrangement.[11] The special electron-deficient 2*c*-5/3*e* B-B bond model, which consists of 2*c*-1*e* and 2*c*-2*e* inter-icosahedral bonds, has been reported in stoichiometric $B_{13}C_2$.[12] The family of boron and boron-rich compounds possess many diverse and novel properties, such as low density, high hardness and strong thermal stability, stemming from the unique structural and bonding nature.[13-17] A topic of great interest is the exploration of evolution of bonding networks and electronic states in boron-rich compounds by introducing atoms with higher electronegativity (e.g., oxygen) to form new compounds with aggravated electron deficiency of boron atoms.

B_2O, as a typical boron-rich compound, has been widely explored through experimental and theoretical investigations, and pressure has been employed to modulate its crystal structures and

electronic properties. B_2O can be regarded as an isoelectronic and asymmetrical analogue of carbon, [18] and has been long assumed to adopt diamond-like and graphite-like structures.[19,20] Graphite-like and diamond-like B_2O samples have been synthesized under high-pressure and high-temperature conditions through the chemical reactions of B_2O_3 with boron and BP with oxygen, respectively. Our recent theoretical prediction solved the crystal structure of the synthesized network of B_2O, and identified a metastable tetragonal phase with a space group of $P4_2mc$ that contains both sp^3- and sp^2-hybridized boron atoms, in contrast to the previously proposed diamond-like structure.[21] Although several structural models have been proposed for B_2O, the evolution of the novel bonding networks and electronic states of the B_2O compound has not been fully explored.

In the present work, we have carried out extensive crystal structure search employing advanced global structural optimization methods in conjunction with first-principles total-energy calculations to explore new structural phases of B_2O stabilized at ambient or elevated pressure conditions. Our computational studies have identified an orthorhombic phase in *Cmmm* symmetry containing B_{12} icosahedral units that is energetically stable at ambient pressure. Under hydrostatic pressure, the orthorhombic phase transforms into a pseudo-layered trigonal phase in *P*-3 symmetry above 1.9 GPa. Calculated electronic band structures indicate that both the *Cmmm* and *P*-3 phases of B_2O are metallic, and they become superconducting at 6.4 K and 5.9 K, respectively.

II. Computational details

The crystal structure searches in the present work are conducted using two recently developed algorithms, namely the CALYPSO (Crystal structure AnaLYsis by Particle Swarm Optimization) code[22] and AIRSS (ab initio random structure searching) code[23,24] based on a global minimization of free energy surfaces. The effectiveness of these advanced search methods have been demonstrated by their recent successful applications in predicting a diverse variety of material structures. [25-38] Ab initio structural relaxation and electronic band structure calculations are carried out using density functional theory (DFT) with the Perdew-Burke-Ernzerh (PBE) parameterization of the generalized gradient approximation (GGA)[39] and PBE-GGA with van der Waals[40] interactions as implemented in the VASP code.[41] The electron-ion interaction is described by the projector-augmented wave (PAW) method,[42] where the $2s^22p^1$ and $2s^22p^4$ electrons ware taken as the valence electrons for B and O atoms, respectively, from the VASP library. The cutoff energy of plane wave functions are set to 500 eV and 800 eV, and the Monkhorst-Pack (MP)[43] k-point meshes with a grid of $2\pi \times 0.06$ Å^{-1} and $2\pi \times$

0.03 $Å^{-1}$ for Brillouin zone sampling are chosen in the structure search and subsequent calculations, respectively. The total-energy calculations have achieved the convergence of less than 1 meV/atom. The phonon dispersions are computed based on the supercell approach using the Phonopy code.[44] The Bader atoms-in-molecules (AIM) analysis is performed using the program InteGrity. Both the atomic core and pseudovalence charge densities are explicitly included. Electron-phonon coupling (EPC) calculations are performed using the plane-wave pseudopotential method and density-functional perturbation theory as implemented in the Quantum-ESPRESSO package.[45] To ensure proper convergence, a 4 × 4 × 4 MP *q*-point mesh and a 12 × 12 × 12 MP *k* mesh are chosen for the *Cmmm* phase, and a 6 × 6 × 4 MP *q*-point mesh and an 18 × 18 × 12 MP *k* mesh are chosen for the *P*-3 phase in the first Brillouin zone.

III. Results and discussion

To explore the intricate bonding networks and electronic properties of B_2O, the variable-cell structural predictions were performed with simulation cell sizes ranging from 2 to 12 formula units (f.u.) in a wide pressure range of 0-40 GPa. The enthalpy curves (per formula unit) of various structures as a function of pressure with respect to that of the previously identified *C*2/m phase[21] are presented in Fig.1. To estimate the accuracy of different choices of exchange-correlation functionals, we have calculated electronic band structures using the standard PBE-GGA, vdW-DF and PBEsol functionals (see Fig. S1 in Supplemental Material[47]). The results show that the calculated band structures are almost identical, indicating that the electronic properties are insensitive to the choice of exchange-correlation functionals. The most thermodynamically stable structure of B_2O under ambient conditions is an orthorhombic crystal phase with a space group of *Cmmm* (12 f.u. per cell), as shown in Fig. 2a, which is energetically much more stable than those proposed in earlier experimental and theoretical studies that are based on much more limited scopes of structure optimization, characterization and determination. The present optimized structural parameters and inequivalent crystallographic sites are listed in Table 1. In stark contrast to the previously proposed B_2O phases, the *Cmmm* phase is built with molecular-like icosahedral B_{12} clusters bridged by oxygen atoms. In each cluster, 12 vertices are occupied by 12 boron atoms, and the bonding configuration at each site has a sixfold coordination connected with five neighboring boron atoms with varying B-B bond lengths in the range of 1.746-1.859 Å and one neighboring oxygen atom with B-O bond lengths of 1.346 Å and 1.386 Å. The fragment of the *Cmmm* phase can be described as a central B_{12} unit surrounded by 8 B_{12} icosahedrons, and the cohesion between the clusters is provided by *exo*-

polyhedral B-O bonds. Each oxygen atom forms covalent bonds with the adjacent B atoms in two B_{12} units, providing straight and bent B-O-B bridges. In addition, we also plotted in Fig 2b the B_2O structure in *Pmma* symmetry, whose enthalpy is only 0.021 eV/atom higher than that of the *Cmmm* phase, that has very similar bonding configurations as in the *Cmmm* phase.

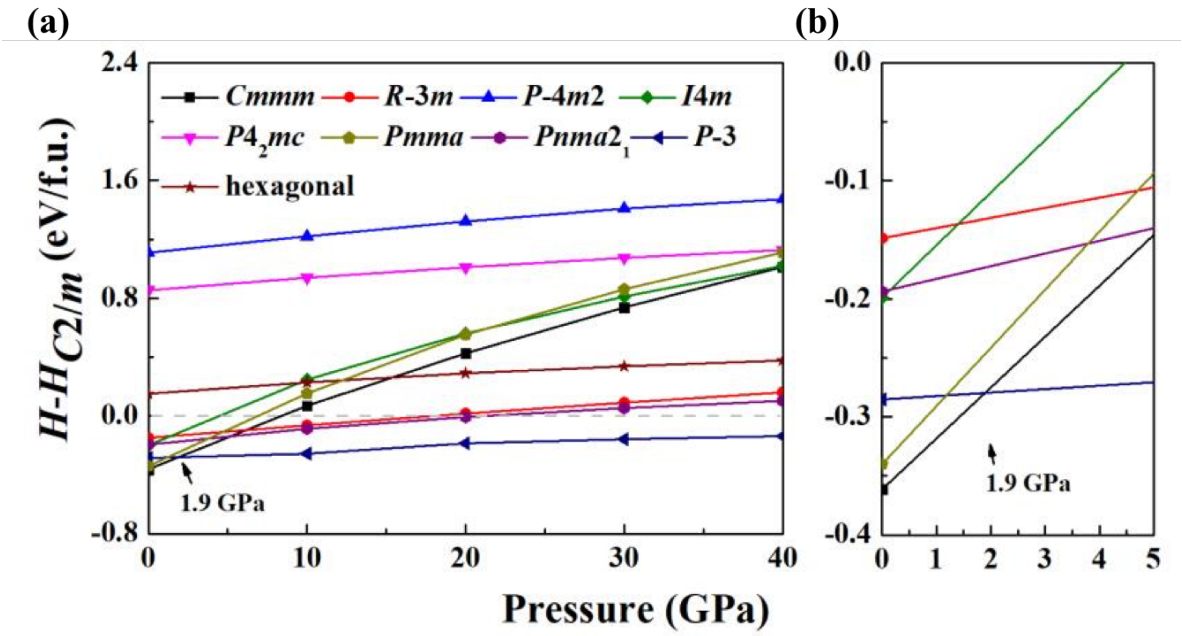

Fig. 1 (a) The relative enthalpy per formula unit as a function of pressure for competing B_2O structures with respect to the previously predicted *C*2/*m* phase. (b) Amplified view of the enthalpy curves for various structures in the pressure range of 0 - 5 GPa.

Our calculations (see Fig. 1) reveal several new B_2O phases at high-pressure conditions, among which a pseudo-layered trigonal *P*-3 phase (6 f.u. per cell) with stacking layers along the packed [001] direction is found to possess the lowest enthalpy above 1.9 GPa. The crystal structure of the *P*-3 phase of B_2O is shown in Fig. 2. From a morphological character view, the B_{12} clusters in the *Cmmm* phase collapse under pressure, leading to a reconstructive transition to a pseudo-layered structure consisting of sandwich-like layers, where the central layer is composed entirely of B with sixfold coordination intercalating into the adjacent layers composed of an equal number of B and O atoms forming a puckered hexagon in the plane for *ab* projection with two inequivalent crystallographic sites for B atoms and an identical site for O atoms. The inequivalent crystallographic sites are listed in Table 1. In a B-O layer model, the coordination of B is four-fold and tetrahedral-based with a sp^3-hybrid unit, in which the tetrahedrons are oriented opposite from both sides of the B-O layer. The lengths of B-B and B-O bonds are shown in Table 2. Based on an

analysis of XRD results, previous experimental studies[19] suggested that the synthesized material should be characterized as a diamond-like structure. Our previous study[21] proposed that the $P4_2mc$ structure is the best candidate for this synthesized B_2O sample. In fact, the $P4_2mc$ structure can be derived by cutting and rearranging the diamond lattice along the [100] crystallographic direction, and thus can be regarded as a defective diamond-like structure. Our current results show that the most stable B_2O structures at ambient conditions (e.g., *Cmmm* and *Pmma*) contain B_{12} icosahedral units that are energetically much superior to the diamond-like or defective diamond-like structures. The calculated enthalpy of the $P4_2mc$ structure is 0.40 eV/atom higher than that of the current *Cmmm* structure. For the entropic effects to overcome the large energy difference, the synthesizing temperatures on the order of 4×10^3 K are needed, unless introducing appropriate chemical reactions, impurities or confinement effect. The diamond-like B_2O might only be synthesized in a very narrow temperature and pressure regime. The disordered structures may be energetically more favorable than the ordered *Cmmm*/*P*-3 structures with the consideration of vibrational and configurational entropy contributions at high temperatures; however, these studies are beyond the scope of this work. Although recent calculations show that the B_2O is slightly above the convex hull,[6] it is noted that our predicted structures are energetically favorable compared with the previously experimental structure.[19,21] We have further examined the phase stability using first-principles molecular dynamic (MD) simulations for the *Cmmm* and *P*-3 phases in the NVT ensemble near the room temperature (300 K). Large supercells with 144 atoms were built for *Cmmm* at 0 GPa and *P*-3 at 2 GPa structures. The fluctuations of the total energy as a function of simulation time (see Fig. S2 in Supplemental Material[47]) show that, after 20 *p*s, there is no structural destruction of the two phases, except for minor thermal fluctuations. To assist further experimental identification of the predicted structural assignments for B_2O, we have simulated x-ray diffraction (XRD) data for the *Cmmm* and *P*-3 phases at 0 and 2 GPa, respectively (see Fig. S3 in Supplemental Material).[47]

Table 1 Optimized structural parameters for the *Cmmm*, *Pmma*, and *P*-3 phases of B_2O.

Space group	Pressure (GPa)	Lattice parameters (Å)	Atom coordinates (fractional)
Cmmm	0	a = 5.533, b = 10.906,	B1 8*q* (0.3422,0.6357,0.5)
		c = 5.466	B2 8*o* (0.2283, 0.5, 0.3347)
		$\alpha = \beta = \gamma$ =90°	B3 8*n* (0.5,0.5808,0.7796)

			O1 4*i* (0, 0.8525, 0)
			O2 4*f* (0.25, 0.75, 0.5)
			O3 4*l* (0, 0.5, 0.7693)
Pmma	0	a = 10.251, b = 5.450	B1 4*j* (0.0114,0.5,0.7842)
		c = 6.249	B2 8*i* (0.0332,0.2216,0.3665)
		$\alpha = \beta = \gamma = 90°$	B3 8*i* (0.1309,0.3358,0.6038)
			B4 4*j* (0.1348,0.5,0.3525)
			O1 4*i* (0.0666,0,0.2665)
			O2 4*k* (0.25,0.2351,0.6671)
			O3 2*b* (0,0.5,0)
			O4 2*f* (0.25,0.5,0.2358)
P-3	2	a = 4.189, c = 7.956	B1 6*g* (0.0045,0.6702,0.7753)
		$\alpha = \beta = 90°$, $\gamma = 120°$	B2 6*g* (0.0971, 0.6912,0.5610)
			O1 6g (0.3353,0.0050,0.8462)

The phonon dispersion curves for the *Cmmm* and *P*-3 phases of B_2O at several selected pressure points have been calculated to check their dynamic stability. The absence of any imaginary phonon frequencies in the entire Brillouin zone demonstrates that the *Cmmm* and *P*-3 phases are dynamically stable, as shown in Fig. 3a and b. The calculated electron localization function (ELF)[48] provides an effective and intuitive analysis of the nature of the electron localization in the bonding structure. Our calculated results shown in Fig. 4a and 4b indicate that a high ELF (> 0.75) can be observed between adjacent B-B and B-O bonds, reflecting the formation of strong covalent bonds in the *Cmmm* and *P*-3 phases. It is noteworthy that lone-pairs remain around oxygen atoms to meet the octet rule, despite the obvious overall electron deficiency in such a boron-rich compound.

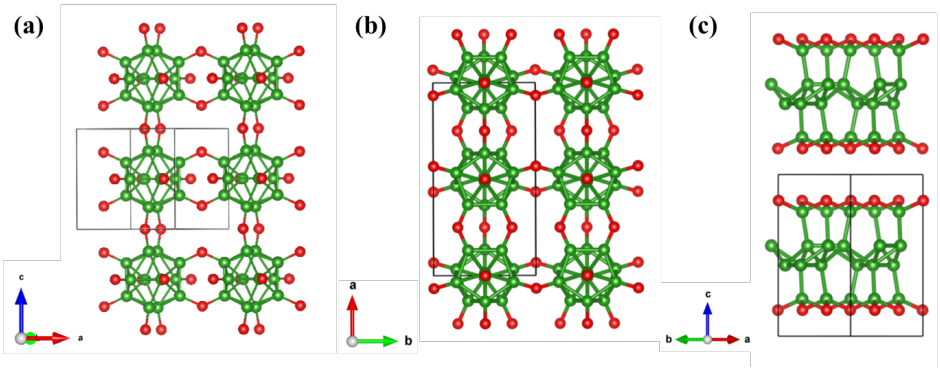

Fig. 2 Predicted crystal structure of (a) the *Cmmm* phase, (b) the *Pmma* phase, and (c) the *P*-3 phase of B_2O. The green balls represent boron, and the red balls represent oxygen.

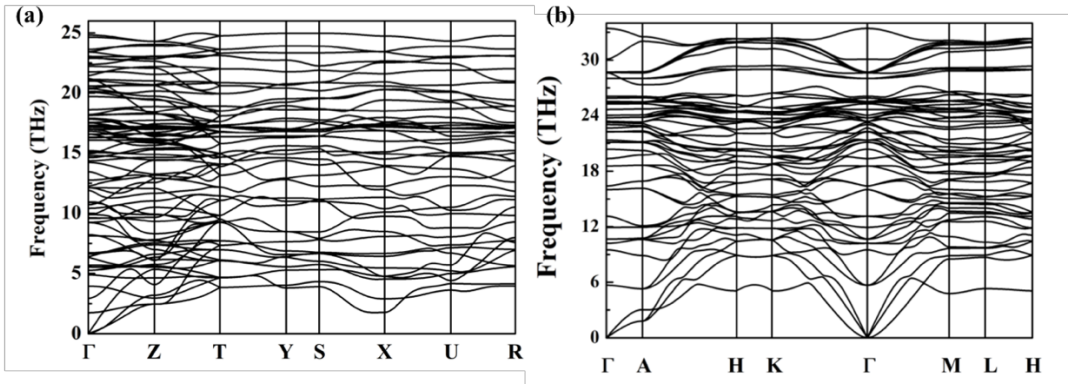

Fig. 3 Calculated phonon dispersions for (a) the *Cmmm* phase at 0 GPa and (b) the *P*-3 phase at 4 GPa.

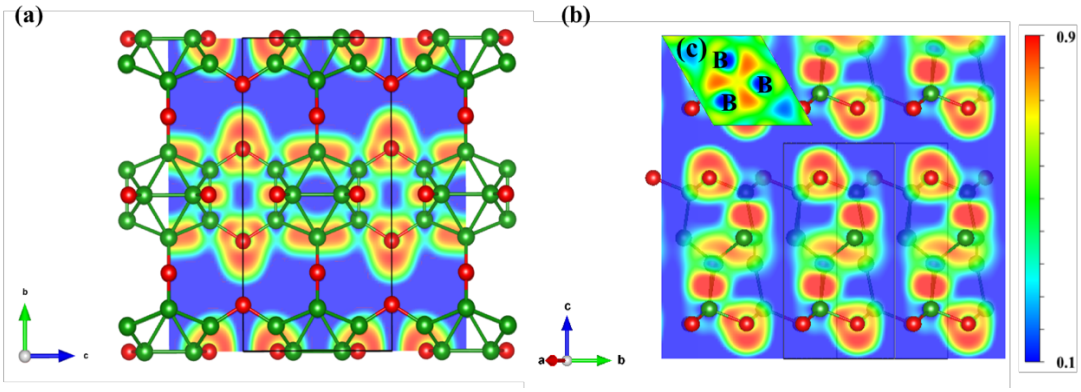

Fig. 4 Calculated ELF plotted in the (100) plane of (a) the *Cmmm* phase at 0 GPa and (b) the *P*-3 phase at 2 GPa.

Having established the crystal structure and stability of the newly identified B_2O phases, we systematically investigate their bonding characters, especially those of the B_{12} icosahedral unit, which are associated with the chemical complexity of boron that is electron deficient but shows nonmetallic character with special multicentral covalent bonds. In particular, we examine the relationship between the number of available valence electrons and the bonding orbitals by forming a large variety of 3*c*-2*e*, 1*e*-2*c* and 5/3*e*-2*c* multicentral bonds in combination with the ubiquitous bonds in polymorphs of boron and boron-rich compounds. Here, we analyze the types of B-B bonds in the B_{12} icosahedral cluster consisting of 12 boron atoms in the *Cmmm* phase. As listed in Table 2, the nearest neighbor distances within a cluster in *Cmmm* B_2O fall in the range of 1.746 to 1.859 Å, which is close to those found in α-B (1.746-1.801 Å) and γ-B_{28} (1.74-1.88 Å), all involving the 2*c*-2*e* and 3*c*-2*e* bonds. Based on Baders' quantum theory of atoms in molecules[49], we have performed a topological analysis of the B-B bonds in the B_{12} icosahedral cluster in the *Cmmm* phase using the bond critical point (BCP) and ring critical point (RCP) with AIM-UC software.[50] The obtained BCP and RCP results reveal the minimum-density point along the bond path and a close path of the bonded atoms, respectively. The values of the electron density and its Laplacian at the BCPs and RCPs are closely related to the properties of the chemical bonds. The presently calculated BCP and RCP of α-B [Table 2] agree with previous theoretical results. We then check the BCPs and RCPs in all the bonds in a *closo*-cluster of B_{12} in the *Cmmm* phase. It is interesting to note that the electron densities of BCPs (ρ_{BCP}) and RCPs (ρ_{RCP}) in the 2*c*-2*e* conventional bonds and 3*c*-2*e* multicenter bonds of the B_{12} unit in the *Cmmm* phase are in the range of 0.78-0.83 and 0.65-0.72 eÅ^{-3}, respectively, which are close to those of α-B (0.73-0.82 and 0.70-0.79 eÅ^{-3}),[11] see Table 2. Furthermore, the calculated $\nabla^2\rho_{CP}$ values for all the intracluster 3*c*-2*e* bonds have negative values, similar to those of α-B, suggesting predominantly covalent features in *Cmmm* B_2O, as illustrated by the typical characteristics of large values of ρ_{BCP} and large negative values of $\nabla^2\rho_{BCP}$. We have further evaluated the chemical bonds in *P*-3 B_2O, as listed in Table 2. From the calculated RCPs, 3*c*-2*e* bonds parallel to the (110) plane appear in the central layer, stemming from the electron-deficient nature of boron. In particular, the theoretical values of $\nabla^2\rho_{RCP}$ for multicenter bonds in the *P*-3 phase are positive, which presents the delocalized nature of electrons throughout the region of the 3*c*-2*e* triangle, as illustrated in Fig. 2c, in stark contrast to the results of α-B and *Cmmm* B_2O. This surprising behavior originates from an unequal electronic donation by the triangular boron atoms, leading to polar-covalent 3*c*-2*e* bonds, which have been reported in γ-B_{28} and $B_{13}C_2$.[11,12]

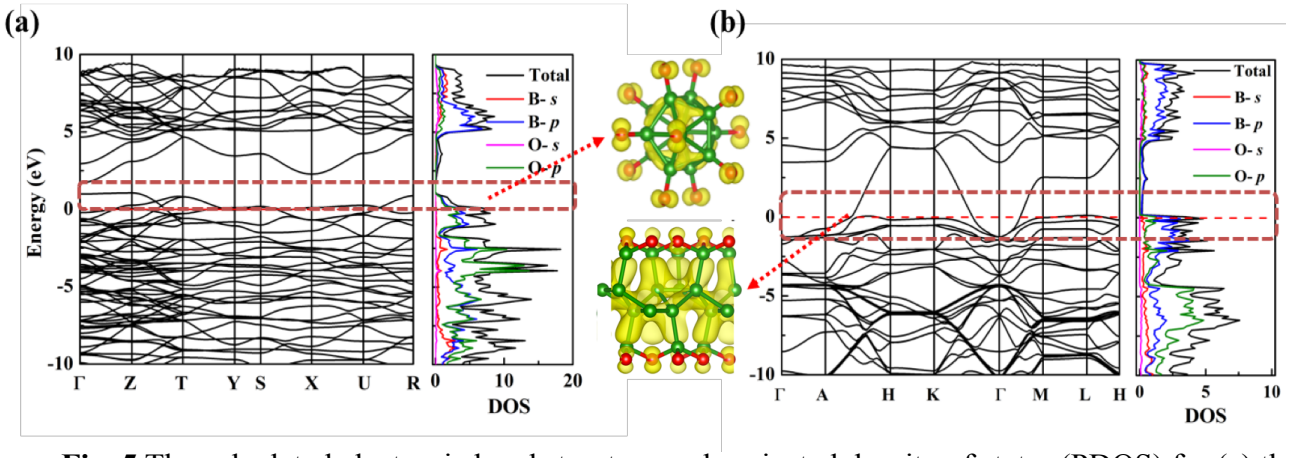

Fig. 5 The calculated electronic band structure and projected density of states (PDOS) for (a) the *Cmmm* phase at 0 GPa and (b) the *P*-3 phase at 2 GPa. The band decomposed charge density near the Fermi level with the isosurface value of 0.01 is shown in the middle panel.

Table 2 The bond distance (Å) and topological properties of electron density for α-B and B_2O.

BOND	D_{BCP}(Å)	P_{CP}(EÅ^{-3})	∇^2P_{CP}(EÅ^{-5})
2*C* AND 3*C* BONDS			
(B1-B1)$_{CMMM}$	**1.7456**	**0.8263**	**-3.4074**
(B2-B2)$_{CMMM}$	**1.7624**	**0.8321**	**-3.4447**
(B3-B3)$_{CMMM}$	**1.8011**	**0.7806**	**-2.7658**
(B1-B1-B2)$_{CMMM}$		**0.7218**	**-1.6591**
(B1-B2-B3)$_{CMMM}$		**0.6531**	**-0.7950**
(B2-B2-B3)$_{CMMM}$		**0.7222**	**-1.5606**
(B3-B3-B1)$_{CMMM}$		**0.7047**	**-1.4011**
(BP-BP)$_{A\text{-}B}$	**1.7461**	**0.8141**	**-2.0753**
(BP-BE)$_{A\text{-}B}$	**1.7928**	**0.7741**	**-2.3951**
(BP-BE)$_{A\text{-}B}$	**1.8005**	**0.7687**	**-2.1387**
(BE-BE)$_{A\text{-}B}$	**1.7784**	**0.7997**	**-2.5729**
(BP-BP-BP)$_{A\text{-}B}$		**0.8139**	**-2.0922**
(BP-BP-BE)$_{A\text{-}B}$		**0.7377**	**-1.2045**
(BP-BE-BE)$_{A\text{-}B}$		**0.7341**	**-1.2440**
(B1-B1-B1)$_{P\text{-}3}$		**0.1322**	**2.2261**
(B2-B2-B2)$_{P\text{-}3}$		**0.6156**	**0.1185**
(B1-B2)$_{P\text{-}3}$	**1.7387**	**0.9907**	**-7.1861**
(B2-B2)$_{P\text{-}3}$	**1.6959**	**0.8692**	**-3.8112**

Borides typically exhibit electron deficiency with nonmetallic characteristics; an effective way to compensate for this is through the formation of multicenter bonds among boron atoms. In the case of α-B, the bonding network possesses 13 internal orbitals with 6 and 20 electrons between 2*c*-2*e* and 3*c*-2*e* bonds, respectively, and 12 external bonding with 4 and 6 electrons between 3*c*-2*e* and 2*c*-2*e*bonds, respectively. For *Cmmm* B_2O, skeleton bonding of the B_{12} unit requires 26 electrons according to the Wade-Jemmis rule.[51,52] A closo-cluster requires 2*n*+2 electrons to stabilize a polycentric bonding system with *n* vertices, which leaves 10 electrons for bonding to neighboring 12 O atoms in the *Cmmm* phase. Since B and O atoms cannot achieve such multicenter bonds, it is not sufficient to form fully occupied conventional 2*c*-2*e* B-O bonds with empty orbitals with aggravated

electron deficiency. The electronic energy band calculation confirms the above analysis by the passage of several bands through the Fermi level [Fig. 5a], suggesting a conducting behavior with holes as major carriers. The theoretical total and projected density of states (DOS) results show the conducting states of the *Cmmm* phase at the Fermi level are mainly derived from the hybridized B-2*p* and O-2*p* orbitals with nearly equal contribution. To understand the particular behavior related to the electron deficiency, the band decomposed charge density distribution near the Fermi level in the energy range of 0-1.8 eV (unoccupied electronic states) has been explored. Our results show that the absence of electrons from full valence band structures are mainly distributed around nonbonding lone-pairs of O and three-center bonds of B atoms. The metallic feature also appears in the *P*-3 phase under high pressure [Fig. 5b]. But unlike in the *Cmmm* phase, the hybridized electronic states near the Fermi level is mainly contributed by B-2*p* orbital in the *P*-3 phase [Fig. 5b].

Superconductivity has been discovered in MgB_2 (T_c = 39 K)[53] and boron-doped diamond[54] (T_c = 4 K) and explored in other covalent compounds[55-57]. Here we examine the electron−phonon coupling (EPC) in the metallic B_2O phases. We have calculated the projected phonon DOS, Eliashberg EPC spectral function $\alpha^2F(\omega)$, and its integral λ for the *Cmmm* phase, and the results are shown in Fig. 6. It is seen that the low vibrational frequencies (below 12 THz) are mainly derived from the O atoms, while the mid-range frequencies (12-38 THz) are mostly contributed by the B_{12} icosahedra stretching modes. The high-frequency vibrations (>40 THz) are mainly associated with the B-O bonding. In contrast to the situation in the *Cmmm* phase, the vibrational modes by the B-O bonding in the *P-3* phase are spread over a wide range of frequency. The superconducting transition temperature T_c is evaluated using the Allen-Dynes modified McMillan equation by the calculated logarithmic average frequency (ω_{log}), Coulomb pseudopotential parameters (μ^*), and EPC integral (λ). Using a the typical μ^* value of 0.1,[58-61] the estimated T_c values are 6.4 K and 5.9 K for the *Cmmm* and *P*-3 phases at 0 and 2 GPa, respectively.

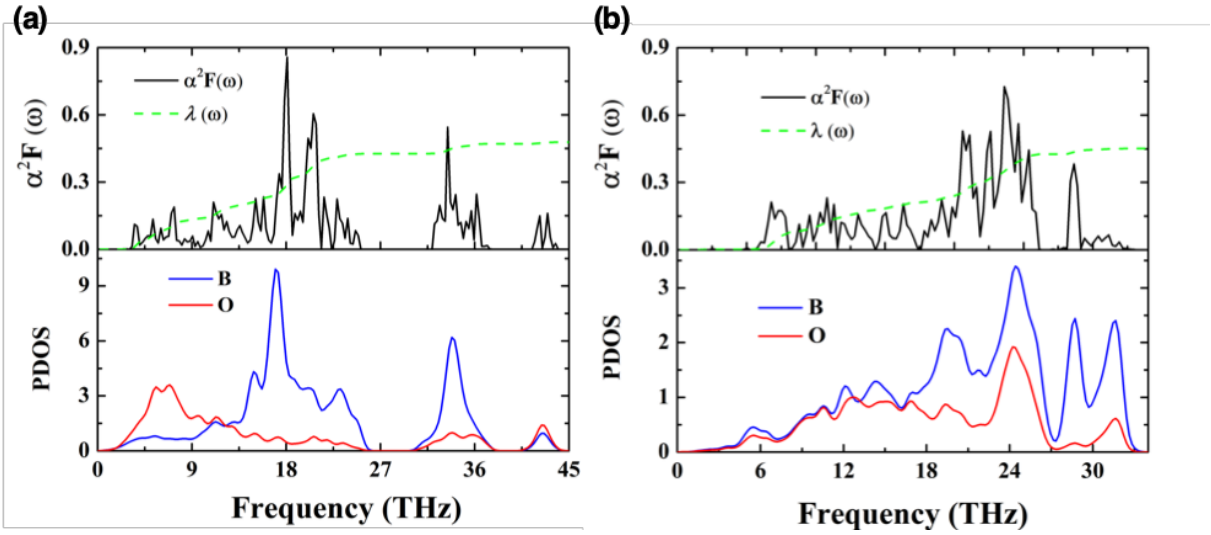

Fig. 6 Calculated projected phonon density of states (PDOS), Eliashberg spectral function $\alpha^2F(\omega)$, and electron-phonon integral for (a) the *Cmmm* phase at 0 GPa and (b) the *P*-3 phase at 2 GPa.

IV. Conclusion

Our computational study has led to the discovery of two new B_2O phases, one in *Cmmm* symmetry at ambient pressure and the other in *P*-3 symmetry above 1.9 GPa. Our systematic investigations have unraveled peculiar bonding characters in these newly identified compounds, especially the evolution of chemical bonds and electronic states associated with the B_{12} icosahedral unit in the *Cmmm* phase and the sandwich-like layers in the *P*-3 phase. Both new phases are metallic with holes as majority carriers for electrical conduction. Electron-phonon coupling calculations show that the *Cmmm* and *P*-3 phases are both superconductors with the transition temperature T_c of about 6.4 K and 5.9 K, respectively. The present findings are expected to simulate experimental studies to synthesize and further explore these new compounds for better fundamental understanding and potential applications.

Conflicts of interest

There are no conflicts to declare.

Acknowledgements

This research was supported by the Natural Science Foundation of China under Nos. 11622432, 11474125, and 11534003; the National Key Research and Development Program of China under

Grant No. 2016YFB0201200 and Program for JLU Science and Technology Innovative Research Team. Parts of the calculations were performed in the High-Performance Computing Center of Jilin University. C. J. P. is supported by the Royal Society through a Royal Society Wolfson Research Merit award and by the EPSRC through grant EP/P022596/1.

*Corresponding author, e-mail:

e-mail: liquan777@jlu.edu.cn,

e-mail: mym@jlu.edu.cn

References

1 B. Albert and H. Hillebrecht, *Angew. Chem. Int. Ed.*, 2009, **48**, 8640–8668.
2 Vladislav Domnich, Sara Reynaud, Richard A Haber and M. Chhowalla, *J. Am. Ceram. Soc.*, 2011, **94**, 3605–3628.
3 H. Hubert, B. Devouard, L. A. J. Garvie, M. OKeeffe, P. R. Buseck, W. T. Petuskey and P. F. McMillan, *Nature*, 1998, **391**, 376–378.
4 X. Guo, J. He, Z. Liu, Y. Tian, J. Sun and H.-T. Wang, *Phys. Rev. B*, 2006, **73**, 104115.
5 D. Emin, *Phys. Today*, 1987, **40**, 55–62.
6 H. Dong, A. R. Oganov, V. V. Brazhkin, Q. Wang, J. Zhang, M. M. D. Esfahani, X. Zhou, F. Wu and Q. Zhu, *Phys. Rev. B*, 2018, **98**, 174109.
7 X. Zhou, A. R. Oganov, X. Shao, Q. Zhu and H. Wang, *Phys. Rev. Lett.*, 2014, **113**, 176101–5.
8 H. Dong, A. R. Oganov, Q. Wang, S. Wang, Z. Wang, J. Zhang, M. M. D. Esfahani, X.-F. Zhou, F. Wu and Q. Zhu, *Sci. Rep.*, 2016, **6**, 31288.
9 M. Fujimori, T. Nakata, T. Nakayama, E. Nishibori, K. Kimura, M. Takata and M. Sakata, *Phys. Rev. Lett.*, 1999, **82**, 4452–4455.
10 S. Mondal, S. van Smaalen, G. Parakhonskiy, S. J. Prathapa, L. Noohinejad, E. Bykova, N. Dubrovinskaia, D. Chernyshov and L. Dubrovinsky, *Phys. Rev. B*, 2013, **88**, 024118–8.
11 S. Mondal, S. van Smaalen, A. Schönleber, Y. Filinchuk, D. Chernyshov, S. I. Simak, A. S. Mikhaylushkin, I. A. Abrikosov, E. Zarechnaya, L. Dubrovinsky and N. Dubrovinskaia, *Phys. Rev. Lett.*, 2011, **106**, 215502.
12 S. Mondal, *Chem. Mater.*, 2017, **29**, 6191–6194.
13 R. J. Nelmes, J. S. Loveday, D. R. Allan, J. M. Besson, G. Hamel, P. Grima and S. Hull, *Phys. Rev. B*, 1993, **47**, 7668–7673.
14 A. Masago, K. Shirai and H. Katayama-Yoshida, *Phys. Rev. B*, 2006, **73**, 104102.
15 D. He, Y. Zhao, L. Daemen, J. Qian, T. D. Shen and T. W. Zerda, *Appl. Phys. Lett.*, 2002, **81**, 643–645.
16 C. Chen, D. He, Z. Kou, F. Peng, L. Yao, R. Yu and Y. Bi, *Adv. Mater.*, 2007, **19**, 4288–4291.

17 J. Liu, S. Wen, Y. Hou, F. Zuo, G. J. O. Beran and P. Feng, *Angew. Chem. Int. Ed.*, 2013, **52**, 3241–3245.
18 H. T. Hall, *Science*, 1965, **148**, 1331–1333.
19 T. Endo, T. Sato and M. Shimada, *J. Mater. Sci. Lett.*, 1987, **6**, 683–685.
20 H. T. Hall and L. A. Compton, *Inorg. Chem.*, 2002, **4**, 1213–1216.
21 Q. Li, W. Chen, Y. Xia, Y. Liu, H. Wang, H. Wang and Y. Ma, *Diamond Relat. Mater.*, 2011, **20**, 501–504.
22 Y. Wang, J. Lv, L. Zhu, S. Lu, K. Yin, Q. Li, H. Wang, L. Zhang and Y. Ma, *J. Phys.: Condens. Matter*, 2015, **27**, 203203–14.
23 C. J. Pickard and R. J. Needs, *Phys. Rev. Lett.*, 2006, **97**, 045504–4.
24 C. J. Pickard and R. J. Needs, *J. Phys.: Condens. Matter*, 2011, **23**, 053201–24.
25 L. Zhang, Y. Wang, J. Lv and Y. Ma, *Nat. Rev. Mater.*, 2017, **2**, 17005.
26 A. Zunger, *Nat. Rev. Chem.*, 2018, **2**, 1–16.
27 J. Lv, Y. Wang, L. Zhu and Y. Ma, *Phys. Rev. Lett.*, 2011, **106**, 015503–4.
28 L. Zhu, H. Liu, C. J. Pickard, G. Zou and Y. Ma, *Nat. Chem.*, 2014, **6**, 644–648.
29 L. Zhu, H. Wang, Y. Wang, J. Lv, Y. Ma, Q. Cui, Y. Ma and G. Zou, *Phys. Rev. Lett.*, 2011, **106**, 2051–4.
30 D. Zhou, Q. Li, Y. Ma, Q. Cui and C. Chen, *J. Phys. Chem. C*, 2013, **117**, 12266–12271.
31 Q. Li, D. Zhou, W. Zheng, Y. Ma and C. Chen, *Phys. Rev. Lett.*, 2013, **110**, 136403–5.
32 M. Zhang, H. Liu, Q. Li, B. Gao, Y. Wang, H. Li, C. Chen and Y. Ma, *Phys. Rev. Lett.*, 2015, **114**, 015502–5.
33 Q. Li, D. Zhou, W. Zheng, Y. Ma and C. Chen, *Phys. Rev. Lett.*, 2015, **115**, 185502–5.
34 D. Zhou, Q. Li, W. Zheng, Y. Ma and C. Chen, *Phys. Chem. Chem. Phys.*, 2017, **19**, 4560–4566.
35 C. Lu, Q. Li, Y. Ma and C. Chen, *Phys. Rev. Lett.*, 2017, **119**, 115503–6.
36 C. Lu and C. Chen, *J. Phys. Chem. Lett.*, 2018, **9**, 2181–2185.
37 C. Lu, M. Amsler and C. Chen, *Phys. Rev. B*, 2018, **98**, 054102.
38 G. Liu, Z. Yu, H. Liu, S. A. T. Redfern, X. Feng, X. Li, Y. Yuan, K. Yang, N. Hirao, S. I. Kawaguchi, X. Li, L. Wang and Y. Ma, *J. Phys. Chem. Lett.*, 2018, **9**, 5785–5791.
39 J. P. Perdew, K. Burke and M. Ernzerhof, *Phys. Rev. Lett.*, 1996, **77**, 3865–3868.
40 M. Dion, H. Rydberg, E. Schröder, D. C. Langreth and B. I. Lundqvist, *Phys. Rev. Lett.*, 2004, **92**, 246401.
41 G. Kresse and J. Furthmüller, *Phys. Rev. B*, 1996, **54**, 11169–11186.
42 G. Kresse and D. Joubert, *Phys. Rev. B*, 1999, **59**, 1758–1775.
43 H. J. Monkhorst and J. D. Pack, *Phys. Rev. B*, 1976, **13**, 5188–5192.
44 A. Togo, F. Oba and I. Tanaka, *Phys. Rev. B*, 2008, **78**, 134106.
45 P. Giannozzi, S. Baroni, N. Bonini, M. Calandra, R. Car, C. Cavazzoni, D. Ceresoli, G. L. Chiarotti, M. Cococcioni, I. Dabo, A. Dal Corso, S. de Gironcoli, S. Fabris, G. Fratesi, R. Gebauer, U. Gerstmann, C. Gougoussis, A. Kokalj, M. Lazzeri, L. Martin-Samos, N. Marzari, F. Mauri, R. Mazzarello, S. Paolini, A. Pasquarello, L. Paulatto, C. Sbraccia, S. Scandolo, G. Sclauzero, A. P. Seitsonen, A. Smogunov, P. Umari and R. M. Wentzcovitch, *J. Phys.: Condens. Matter*, 2009, **21**, 395502–20.
46 J. P. Perdew, A. Ruzsinszky, G. I. Csonka, O. A. Vydrov, G. E. Scuseria, L. A. Constantin, X. Zhou and K. Burke, *Phys. Rev. Lett.*, 2008, **100**, 136406.
47 See Supplemental Material for additional results on calculated electronic band structures, fluctuations of potential energies as a function of the molecular dynamic simulation step, simulated XRD and structural details for the newly predicted B_2O phases.

48 B. Silvi and A. Savin, *Nature*, 1994, **371**, 683–686.
49 R. F. W. Bader, *Atoms in Molecules*, 2002.
50 D. Vega and D. Almeida, *J. Comput. Methods Sci. Eng.*, 2014, **14**, 131–136.
51 E. D. Jemmis, M. M. Balakrishnarajan and P. D. Pancharatna, *J. Am. Chem. Soc.*, 2001, **123**, 4313–4323.
52 K. Wade, *Adv. Inorg. Chem. Radiochem.*, 1976, **18**, 1–66.
53 P. P. Singh, *Phys. Rev. Lett.*, 2006, **97**, 247002.
54 E. A. Ekimov, V. A. Sidorov, E. D. Bauer, N. N. Melnik, N. J. Curro, J. D. Thompson and S. M. Stishov, *Nature*, 2004, **428**, 542–545.
55 Q. Li, H. Wang, Y. Tian, Y. Xia, T. Cui, J. He, Y. Ma and G. Zou, *J. Appl. Phys.*, 2010, **108**, 023507–6.
56 H. Liu, Q. Li, L. Zhu and Y. Ma, *Phys. Lett. A*, 2011, **375**, 771–774.
57 K. Xia, M. Ma, C. Liu, H. Gao, Q. Chen, J. He, J. Sun, H. Wang, Y. Tian and D. Xing, *Mater. Today Phys.*, 2017, **3**, 76–84.
58 L. Boeri, J. Kortus and O. K. Andersen, *Phys. Rev. Lett.*, 2004, **93**, 34–4.
59 X. Zhong, H. Wang, J. Zhang, H. Liu, S. Zhang, H.-F. Song, G. Yang, L. Zhang and Y. Ma, *Phys. Rev. Lett.*, 2016, **116**, 73–6.
60 J. Wang, X. Song, X. Shao, B. Gao, Q. Li and Y. Ma, *J. Phys. Chem. C*, 2018, **122**, 27820–27828.
61 H. Zhai, Z. Qin, D. Sun, J. Wang, C. Liu, N. Min and Q. Li, *Phys. Chem. Chem. Phys.*, 2018, **20**, 23656–23663.